



Gravity and Magnetic Investigations of the Mojave National Preserve and Adjacent Areas, California and Nevada

By V.E. Langenheim, S. Biehler, R. Negrini, K. Mickus, D.M. Miller, and R.J. Miller

Prepared in cooperation with National Park Service



View looking south from Lanfair Valley towards the Woods Mountains (photograph by V.E. Langenheim)

Open-File Report 2009-1117

**U.S. Department of the Interior
U.S. Geological Survey**

U.S. Department of the Interior
KEN SALAZAR, Secretary

U.S. Geological Survey
Suzette M. Kimball, Acting Director

U.S. Geological Survey, Reston, Virginia 2009

For product and ordering information:
World Wide Web: <http://www.usgs.gov/pubprod>
Telephone: 1-888-ASK-USGS

For more information on the USGS—the Federal source for science about the Earth, its natural and living resources, natural hazards, and the environment:
World Wide Web: <http://www.usgs.gov>
Telephone: 1-888-ASK-USGS

Suggested citation:
Langenheim, V.E., Biehler, S., Negrini, R., Mickus, K., Miller, D.M., and Miller, R.J., 2009, Gravity and magnetic Investigations of the Mojave National Preserve and adjacent areas, California and Nevada: U.S. Geological Survey Open-File Report 2009-1117, 25 p. [<http://pubs.usgs.gov/of/2009/1117/>].

Any use of trade, product, or firm names is for descriptive purposes only and does not imply endorsement by the U.S. Government.

Although this report is in the public domain, permission must be secured from the individual copyright owners to reproduce any copyright the material contained within this report.

Contents

Abstract.....	1
Introduction	1
Acknowledgments.....	2
Gravity data	2
Aeromagnetic data.....	4
Physical property data.....	4
Methods	5
Geophysical boundaries.....	5
Depth to basement.....	6
Discussion	8
Conclusions and recommendations.....	11
References Cited	11

Figures

1. Index map of the study area	16
2. Simplified geologic map of the study area.....	17
3. Map of gravity measurements in the study area	18
4. Map and photograph of secondary gravity base station	19
5. Isostatic gravity map of the study area	20
6. Isostatic gravity contours on simplified geologic map	21
7. Aeromagnetic map of study area	22
8. Basin depth from inversion of gravity data	23
9. Bedrock gravity map of the study area	24
10. Magnetization boundaries in the study area	25

Tables

1. Aeromagnetic-survey specifications	4
2. Drill holes	7
3. Density-depth functions for basin-filling deposits	8

Abstract

Gravity and aeromagnetic data provide the underpinnings of a hydrogeologic framework for the Mojave National Preserve by estimating the thickness of Cenozoic deposits and locating inferred structural features that influence groundwater flow. An inversion of gravity data indicates that thin (<1 km) basin deposits cover much of the Preserve, except for Ivanpah Valley and the Woods Mountains volcanic center. Localized areas of Cenozoic deposits thicker than 500 m are predicted beneath parts of Lanfair Valley, Fenner Valley, near Kelso, Soda Lake, and southeast of Baker. Along the southern margin of the Mojave National Preserve, basins greater than 1 km deep are located between the Clipper and Marble Mountains, between the Marble and Bristol Mountains, and south of the Bristol Mountains near Amboy. Both density and magnetization boundaries defined by horizontal-gradient analyses coincide locally with Cenozoic faults and can be used to extend these faults beneath cover. Magnetization boundaries also highlight the structural grain within the crystalline rocks and may serve as a proxy for fracturing, an important source of permeability within the generally impermeable basement rocks, thus mapping potential groundwater pathways through and along the mountain ranges in the study area.

Introduction

The Mojave National Preserve encompasses approximately 1.5 million acres within the northeastern Mojave Desert, a large physiographic province primarily defined by its Neogene geologic history (fig. 1). The desert physiography consists of ranges that are separated by valleys filled by either a thick section of alluvial materials or underlain at shallow depths by pediments; it is the basins filled with porous alluvial deposits that presumably store most of the groundwater resources in the Preserve. Outside the Preserve, groundwater resources are increasingly sought after for consumptive uses, given the scarcity of surface water and a growing population in southern California and Nevada (Schmidt and Webb, 2001). Here we present new gravity data, compiled with existing gravity and aeromagnetic data, to determine basin geometries, infer structural features that may influence groundwater flow, and estimate depth to pre-Cenozoic rocks or bedrock. Characterizing the hydrogeologic framework will contribute to the estimation of the quantity of groundwater in storage and promote an understanding of hydraulic connectivity between areas subject to groundwater drawdown and water resources within the Preserve.

This study builds upon a recently published report that focused on the mineral-resource potential of the Mojave National Scenic Area (Theodore, 2007), and it covers the same area as the Mojave National Preserve. We utilized a geologic map (Miller and others, 2007a), as well as gravity and aeromagnetic data (Mariano and others, 2007a,b) compiled for that study. We expanded the study area of Theodore (2007) beyond the Preserve boundaries, incorporating surrounding ranges and basins where groundwater development may affect the hydrology of the Preserve (fig. 1). Additional gravity data were collected in October 2006 to augment sparse measurements in the Fenner and Lanfair Valleys.

The study area includes ranges that transect the Preserve from the Granite Mountains in the southeast to the Ivanpah and New York Mountains in the northeast. These ranges are as high as 2,000 m (fig. 1) and are underlain by basement rocks that are

as old as early Proterozoic and as young as Cretaceous (fig. 2). The rest of the Preserve is characterized by gentler topography, exemplified by the pediment dome centered near Cima. Although the basement rocks have experienced episodes of metamorphism and plutonism during the Proterozoic and Mesozoic (Theodore, 2007), shortening during the middle to late Mesozoic, and extension during the late Cretaceous (Miller and others, 1996; Wells and others, 2005), the rocks in the Preserve (except for the northern and southeastern parts) largely escaped the significant Miocene extensional deformation that occurred in metamorphic core complexes to the east along the Colorado River corridor (in the Sacramento Mountains) and to the southwest in the central Mojave Desert (Theodore, 2007). Instead, along the southern and eastern margins of the Preserve, Miocene volcanism was widespread where it blanketed pediments (Miller, 1995). During the late Miocene, extensive erosion produced broad pediment domes in the northwestern part of the preserve, which was followed by alkali-basaltic volcanism of the Cima volcanic field. Erosion of the pediment domes and mountain ranges continues to supply sediments to the adjacent valleys. The Preserve today is relatively tectonically quiescent, as exemplified by the relative absence of seismicity compared to the southwestern part of the study area, which experienced aftershocks of the 1999 Hector Mine earthquake (fig. 1).

The diverse geologic history of the Preserve has led to contrasts in density and magnetic properties among these rock types that create measurable gravity and magnetic anomalies, which in turn can be modeled to determine the geometry of the rock masses. Here we present a revised gravity map of the study area based on new data, a compilation of aeromagnetic data for the area with magnetization boundaries that reflect lithologic and structural features, and an inversion of the gravity data used to estimate thickness of Cenozoic deposits.

Acknowledgments

We would like to thank Geoff Phelps and Dave Ponce (U.S. Geological Survey, Menlo Park, Calif.) for their review comments and suggestions. Debra Hughson (National Park Service, Barstow, Calif.) provided invaluable information on well data and helped coordinate access to the Preserve. We also thank Anne Elston for assistance in making some of the physical-property measurements. This study was funded by the National Cooperative Geologic Mapping Program and the National Park Service.

Gravity Data

The gravity data in this report consist of 181 new stations concentrated in the southeastern part of the Preserve and study area (“USGS, this study”, fig. 3). The new measurements were along roads and were tied to primary base station PB1309A at lat 34°39.22'N. and long 116°00.81'W. (NAD27) with an observed gravity value of 979,521.255 mGal (Roberts and Jachens, 1986). A secondary base station was established in Ludlow at lat 34°43.39'N. and long 116°09.79'W., with an observed gravity value of 979,506.32 ± 0.02 mGal (fig. 4).

These data were combined with pre-existing gravity data, which included previously published data shown in Roberts and others (1990) and data collected or compiled since then. Data include 85 gravity stations collected by the U.S. Geological Survey (USGS; fig. 3) before 2006 (C. Roberts, written commun., 2000); 1,081 stations compiled or collected by University of California, Riverside (UCR, fig. 3); 743 National Geodetic Survey stations (NGS; fig. 3); 222 stations collected by Kevin Mickus; 280

stations from Acord (1989); 228 stations collected by California State University, Bakersfield (CSUB; fig. 3); and 432 stations from Carlisle (1982). Gravity stations are nonuniformly distributed in the region (fig. 3). Most of the data are along roads, and there is sparse coverage in the more mountainous and remote areas (<0.5 stations per km²).

The new gravity data were reduced using standard gravity methods (Blakely, 1995) and include the following corrections: (1) the earth-tide correction, which corrects for tidal effects of the moon and sun; (2) instrument-drift correction, which compensates for drift in the instrument's spring; (3) the latitude correction, which incorporates the variation of the Earth's gravity with latitude; (4) the free-air correction, which accounts for the variation in gravity due to elevation relative to sea level; (5) the Bouguer correction, which corrects for the attraction of material between the station and sea level; (6) the curvature correction, which corrects the Bouguer correction for the effect of the Earth's curvature; (7) the terrain correction, which removes the effect of topography to a radial distance of 167 km (104 mi); and (8) the isostatic correction, which removes long-wavelength variations in the gravity field inversely related to topography.

Conversion of meter readings to gravity units was made using factory calibration constants, as well as a secondary calibration factor determined by multiple gravity readings over the Mt. Hamilton calibration loop east of San Jose, California (Barnes and others, 1969). The gravity meter used in this survey, LaCoste and Romberg G17C, has a secondary calibration factor of 1.00078. Observed gravity values were based on a time-dependent linear drift between successive base readings and were referenced to the International Gravity Standardization Net 1971 gravity datum (Morelli, 1974, p. 18). Free-air gravity anomalies were calculated using the Geodetic Reference System 1967 formula for theoretical gravity on the ellipsoid (International Union of Geodesy and Geophysics, 1971, p. 60) and Swick's formula (Swick, 1942, p. 65) for the free-air correction. Bouguer, curvature, and terrain corrections were added to the free-air anomaly to determine the complete Bouguer anomaly at a standard reduction density of 2,670 kg/m³. Finally, a regional isostatic gravity field was removed from the Bouguer field assuming an Airy-Heiskanen model for isostatic compensation of topographic loads (Jachens and Roberts, 1981) with an assumed crustal thickness of 25 km (16 mi), a crustal density of 2670 kg/m³, and a density contrast across the base of the model of 400 kg/m³. Gravity values are expressed in mGal, a unit of acceleration or gravitational force per mass equal to 10⁻⁸ km/s². Gravity data were gridded at an interval of 300 m using a computer program (Webring, 1981) based on a minimum curvature algorithm by Briggs (1974) and displayed as a color-contoured map (fig. 5) and as contours on a simplified geologic map (fig. 6).

Station locations and elevations were obtained using a Trimble differential Global Positioning System instrument with the GeoExplorer CE handheld receiver. The GeoExplorer CE receiver uses Wide Area Augmentation System correction messages, which, combined with base station post-processing, results in submeter vertical accuracy.

Terrain corrections, which account for the variation of topography near a gravity station, were computed using a combination of manual and digital methods. Terrain corrections consist of a three-part process: (1) the innermost or field terrain correction, (2) inner-zone terrain correction, and (3) outer-zone terrain correction. Field-terrain corrections were estimated in the field and extend from the station to a radial distance of 68 m (223 ft), equivalent to Hayford and Bowie's (1912) zone B. Inner-zone terrain corrections were estimated from 10- or 30-m resolution Digital Elevation Models (DEMs) derived from USGS 7.5' topographic maps, and extend from 68 m (223 ft) to a radial distance of 590 m (D. Plouff, USGS, unpublished software, 2005). Outer-zone

terrain corrections, to a radial distance of 167 km (104 mi), were computed using a DEM derived from USGS 1:250,000-scale topographic maps and an automated procedure (Plouff, 1966; Plouff, 1977; Godson and Plouff, 1988). Digital terrain corrections are calculated by computing the gravity effect of each grid cell by using the distance and difference in elevation of each grid cell from the gravity station.

Aeromagnetic Data

Regional aeromagnetic data were compiled to produce an aeromagnetic map of the study area. Aeromagnetic data consist of several regional surveys flown at various altitudes and flightline spacings (table 1). Flightline spacing ranged from 800 m (0.5 mi) to 4,800 m (3 mi), and flight elevations ranged from 120 m (400 ft) above the ground surface to 305 m (1,000 ft) constant altitude. The regional data were adjusted to a common datum and then merged by smooth interpolation across survey boundaries to produce an aeromagnetic map of the area (fig. 7). All but the westernmost part of the Mojave National Preserve is covered by relatively detailed data (flightline spacing of 800 m).

Table 1. Aeromagnetic-survey specifications, Mojave National Preserve, California and Nevada

Name	Flightline spacing, in meters	Flightline direction	Altitude in meters	Year flown	Reference
Kingman-Trona	800	E-W	305	1981	USGS (1983)
Needles	800	E-W	305	1980	USGS (1981)
Southern Nevada	1600	E-W	305	1978-79	USGS (1979)
San Bernardino	1600	E-W	120	1979-80	High Life (1980)
Twentynine Palms	1600	N-S	305	1982	Roberts and Jachens (1999)
Trona, CA	4800	E-W	120	1978	GeoLife Inc. (1979)

Physical Property Data

Density and magnetic properties of rock samples are used for gravity and magnetic modeling, as well as a guide for gravity-inversion calculations. Rock samples from existing collections at the USGS were measured for densities and magnetic susceptibilities. Magnetic susceptibility, along with density and rock identification, accompany this report.

Rock samples from existing collections at the USGS were measured for densities and magnetic susceptibilities. Densities were determined using a precision Sartorius electronic balance. All rocks were weighed dry in air (W_a), saturated in water (W_w), and saturated with water in air (W_s). From these measurements, grain density, dry bulk density, and saturated bulk density were calculated using the following formulas:

$$\text{Grain density } (D_1) = W_a / (W_a - W_s)$$

$$\text{Dry bulk density } (D_2) = W_a / (W_s - W_w)$$

$$\text{Saturated bulk density } (D_3) = W_s / (W_s - W_w)$$

Magnetic susceptibilities (k) were measured using a Geophysica KT-5 susceptibility meter and are reported from 0.01 to 0.1×10^{-3} SI units. The Geophysica KT-5 calculates volume susceptibility by assuming the sample shape is an infinite half-space. The instrument's ability to measure magnetic susceptibility is affected by surface

roughness, weathering, and sample size, all of which can result in an underestimation of a sample's true susceptibility. The magnetic-susceptibility values reported represent an average of multiple (4-8) readings on the sample.

These data augment results from wilderness studies (Miller and others, 1986; Wilshire and others, 1987), as well as a report by Chapman and others (1986) on magnetic susceptibilities of the Ivanpah mining district. Acord (1989) also measured densities from a dozen samples in the Soda-Avawatz area. Our data support previous studies that indicate the crystalline basement rocks are denser on average than the Tertiary volcanic rocks (2,670 versus 2,500 kg/m³, respectively), but are characterized by a wide range of densities (2,520 to 3,060 kg/m³). In general, the Cretaceous granitic rocks are less dense than those of Proterozoic or Jurassic age (Hendricks, 2007). Tertiary volcanic rocks are, on average, more magnetic than the other rock types; but the highest measured susceptibility was from a biotite gneiss.

Limited physical-property data exist for sedimentary rocks in the study area, with direct measurements only for rocks of pre-Cenozoic age. These rocks are as dense as other pre-Cenozoic deposits, but are weakly magnetic. These rocks produce low-amplitude magnetic anomalies generally undetectable by airborne surveys, except for carbonate rocks that have been metamorphosed into skarn deposits (Chapman and others, 1986; Hendricks, 2007). Although we have no direct susceptibility measurements for Tertiary sedimentary rocks or deposits, these rocks are most likely less magnetic than Tertiary volcanic rocks or crystalline basement rocks.

The density contrast between bedrock and Cenozoic deposits is important for the depth to basement calculations. No density measurements, however, were made on Quaternary or Tertiary sedimentary deposits for this study because of the difficulty of obtaining direct density measurements on Quaternary and Tertiary sedimentary rocks. One must rely on indirect information from other areas or on other geophysical measurements. The most direct measure of the density of the sedimentary sequence comes from borehole gravity surveys outside the study area, such as those compiled for the State of Arizona (Tucci and others, 1982, their figure 3) and those compiled for the Basin and Range province (Jachens and Moring, 1990). Indirect information on densities of Cenozoic sedimentary rocks comes from sonic velocities measured along seismic-refraction profiles in Ivanpah Valley (Carlisle and others, 1980) and from stacking velocities used in shallow seismic-reflection profiles at the southern end of Fenner Valley (Black, 1997). By using the relation Gardner and others (1974) developed for sedimentary rocks,

$$\rho = 230v^{0.25}, \quad (1)$$

one can estimate the density, ρ (kg/m³), from the sonic velocity, v (ft/s). The seismic-refraction studies indicate a two- or three-layered velocity structure, with calculated densities increasing with depth, from as low as 1,700 to 1,800 kg/m³ within 100 m of the surface to 2,200 to 2,300 kg/m³ at a depth of a few hundred meters.

Methods

Geophysical Boundaries

To better define the edges of geophysical sources and to help derive geophysical lineaments and terranes, the maximum horizontal gradients of both gravity and magnetic data were computer generated. A technique described by Blakely and Simpson (1986) was used to calculate maximum horizontal gradients, which reflect abrupt lateral changes in the density or magnetization of the underlying geology, especially where the sources

are shallow. For example, the horizontal displacement of a gradient maximum from the top edge of an offset horizontal layer is always less than or equal to the depth to the top of the source for moderate to steep dips (45° to vertical) (Grauch and Cordell, 1987). We calculated magnetization boundaries by using aeromagnetic data that were filtered to emphasize shallow sources (top of source <1 km). Alignment of maximum horizontal-gradient locations can be used to define lineaments, faults, and boundaries of geologic features.

Depth to Basement

We used a three-dimensional iterative technique (Jachens and Moring, 1990) to separate the gravity anomaly into a component caused by variations in thickness of the Cenozoic deposits (fig. 8) and a component caused by lateral density variations in the bedrock (fig. 9). The method requires knowledge of the gravity field, exposed geology, and vertical-density variation within the Cenozoic basin deposits. This method does not take into account possible lateral variations in the density distribution of the Cenozoic deposits. Gravity data are separated into observations made on bedrock outcrops and observations made over the basin. A first approximation of the bedrock gravity field is determined by interpolating a smooth surface through all gravity values measured on bedrock outcrops. The basin gravity is the difference between the observed gravity field on the original map and the first approximation of the bedrock gravity field and is used to calculate the first approximation of the thickness of Cenozoic deposits. The thickness is forced to zero where bedrock is exposed. This first approximation of the bedrock gravity is too low near the basin edges because of the effects of the nearby low-density deposits on the bedrock stations. The bedrock gravity-station values are “corrected” for the effects of the low-density deposits (the effects are calculated directly from the first approximation of the thickness of the Cenozoic deposits). and a second approximation of the bedrock gravity field is made by interpolating a smooth surface through the corrected bedrock gravity observations. This iteration leads to an improved estimate of the basin gravity field, an improved depth to bedrock estimate, and a new correction to the bedrock gravity values. This procedure is repeated until successive iterations produce no significant changes in the bedrock gravity field.

This method can use well data or other independent information on the thickness of the Cenozoic deposits to constrain the inversion. A set of 53 drill holes (table 2) with some geologic information was available to constrain the gravity interpretations. Most of these were water wells that were of limited utility because of their generally shallow depth extents (less than 300 m) and because of lithologic descriptions that were challenging to interpret. One key drillhole, (07120050 in table 2, also known as the Ivanpah Partnership “Ivanpah 13”; Division of Oil and Gas, 1980) penetrated to a depth of 1,891 m (6,205 ft) in Ivanpah Valley and helped to constrain the location of a significant bedrock gravity gradient beneath the valley. Given the usual lack of information on the density of the Cenozoic deposits, we assumed a density-depth function derived from borehole gravity surveys in the Basin and Range (table 3; Jachens and Moring, 1990) between the bedrock and the basin fill. This density-depth function may provide an estimate of the minimum thickness. Given the maturity of the landscape, the density of the fill may be higher (more consolidated), and the resulting thickness may be greater, as much as several hundred meters in the deepest basins. Thus, these results provide insight into the shapes of the basins, but can be less effective in estimating the thickness of basin fill, especially in basins having thick basalt flows, or in areas of poor well control.

Table 2. Drill holes used to constrain the depth-to-basement calculation, Mojave National Preserve, California and Nevada

Well ID	Latitude	Longitude	Basin thickness		Total depth	
			(ft)	(m)	(ft)	(m)
07100015 ^a	35.4015°	-116.1478°	100	30	190	58
07120041 ^a	35.4539°	-115.3436°			1,870	570
07120045 ^a	35.4618°	-115.3335°			3,477	1,060
07120050 ^a	35.4067°	-115.2968°			6,502	1,891
5N12E5Z1 ^b	34.5380°	-115.6920°	1,500	457	1,500	457
5N14E15K1 ^b	34.5180°	-115.5000°			425	130
5N14E15L1 ^b	34.5180°	-115.5070°			541	165
5N15E4X1 ^b	34.5520°	-115.4170°			895	273
5N15E4X1 ^b	34.5530°	-115.4160°			888	271
6N11E10F1 ^b	34.6280°	-115.8250°	663	202	681	208
6N11E30X1 ^b	34.5870°	-115.8730°	805	245	1,000	300
7N6E14P1 ^b	34.6920°	-116.3120°			90	27
7N8E8B1 ^b	34.7180°	-116.1600°	760	232	1,600	488
7N9E25Z1 ^b	34.6650°	-116.0000°	242	74	2,275	693
BW#2 ^c	35.2900°	-115.2420°	362	110	457	139
Danby#1 ^c	34.6330°	-115.3430°			637	194
Danby#2 ^c	34.6320°	-115.3440°	758	231	839	258
Fenner#1 ^c	34.8170°	-115.1770°	340	104	800	244
Fenner#2 ^c	34.8160°	-115.1780°	344	105	1,060	323
Goffs#1 ^c	34.9200°	-115.0620°			926	282
Goffs#2 ^c	34.9190°	-115.0630°			960	293
Goffs#3 ^c	34.9190°	-115.0630°			1,123	342
LF#19 ^c	35.1270°	-115.1800°			550	168
LF#20 ^c	35.1180°	-115.1550°			550	168
LF#9 ^c	35.2020°	-115.1980°			879	268
463754 ^d	35.0642°	-115.4053°	360	110	900	274
KELSO#8 ^d	35.0112°	-115.6495°			1,664	507
KELSO#9 ^d	35.0110°	-115.6525°			1,970	600
KELSO#10 ^d	35.0097°	-115.6578°			1,400	427
Thompson ^d	35.4717°	-115.2875°			2,006	611
Ivanpah 1-23 ^d	35.4533°	-115.3450°			2,444	745
13N14W6J1 ^e	35.2375°	-115.5183°			900	274
14N13E10D3 ^e	35.3150°	-115.5833°	63	19	73	22
14N13E10D4 ^e	35.3150°	-115.5833°	67	20	73	22
15N14E24A3 ^e	35.3817°	-115.4308°	620	189	2,825	861
15N14E24A1 ^e	35.3750°	-115.4317°			2,207	673
15N15E13G1 ^e	35.3850°	-115.3267°			530	162
15N15E13G2 ^e	35.3850°	-115.3267°			822	251
15N15E13G3 ^e	35.3850°	-115.3267°			825	251
15N15E56J1 ^e	35.4550°	-115.3883°			735	224
15N15E56J2 ^e	35.4550°	-115.3883°			825	251
15N15E57G1 ^e	35.4583°	-115.3750°			412	126

Table 2 (cont.)

Well ID	Latitude	Longitude	Basin thickness		Total depth	
			(ft)	(m)	(ft)	(m)
15N15E59P1 ^e	35.4533°	-115.3450°			2,210	674
16N15E12Q1 ^e	35.5217°	-115.3133°			506	154
16N15E12Q2 ^e	35.5200°	-115.3125°			588	179
16N15E12Q3 ^e	35.5233°	-115.3135°	602	183	603	184
27S59EP1 ^e	35.6083°	-115.3900°			600	183
28/63-27 ^f	35.4825°	-114.9280°	452	138	452	138
28/63/34 ^f	35.4683°	-114.9255°	75	23	366	112
28/63-35 ^f	35.4678°	-114.9138°			450	137
BW-1 ^g	34.8610°	-116.1890°			504	154
IV-1 ^h	35.4290°	-115.3320°			335	102
SD-1 ⁱ	35.1770°	-116.0580°			415	126

^aDivision of Oil and Gas, 1980.

^bMoyle, 1967.

^cThompson, 1929.

^dD. Hughson, written. commun., 2006.

^eMoyle, 1972.

^fRush and Huxel, 1966.

^gCalzia, 1991a.

^hCalzia, 1991b.

ⁱCalzia, 1991c.

Table 3. Density-depth function¹, Mojave National Preserve, California and Nevada.

Depth Range, in meters	Based on Basin and Range (Jachens and Moring, 1990), in kilograms per cubic meter
0—200	-650
200—600	-550
600—1,200	-350
>1,200	-250

¹Density contrast relative to underlying pre-Cenozoic bedrock.

Discussion

In general, isostatic gravity anomalies reflect lateral (horizontal) density variations in the middle to upper crust (Simpson and others, 1986). Thus, gravity anomalies can be used to infer the subsurface structure of known or unknown geologic features. Gravity anomalies commonly reveal features, such as basement terranes, sedimentary basins, and faults.

One of the most significant density contrasts in the upper crust is that between dense pre-Cenozoic rocks, defined here as bedrock, and Cenozoic lower-density rocks and deposits. The prominent gravity low in Ivanpah Valley (figs. 5, 6) reflects a deep (>1 km) basin, as corroborated by seismic-refraction data (Carlisle and others, 1980) and

drill-hole data (Division of Oil and Gas, 1980). The most prominent gravity low in the study area south of Lanfair Valley reflects a thick accumulation of Tertiary volcanic deposits in the Woods Canyon volcanic center (McCurry, 1988; Mickus and McCurry, 1999).

Not all gravity anomalies, however, reflect a density contrast between pre-Cenozoic basement and younger basin fill or volcanics. For example, gravity values measured on crystalline basement in the Mid Hills and southern New York Mountains are 21-24 mGal lower than those measured on basement in the northern New York Mountains and as much as 33 mGal lower than those measured on Proterozoic rocks in the Ivanpah Mountains. Thus, substantial density variations within the pre-Cenozoic rocks can produce gravity variations that obscure the gravity anomalies of interest for hydrogeologic studies, which are those caused primarily by variations in the thickness of the Cenozoic deposits. The bedrock gravity field (fig. 9) highlights these significant density contrasts between the denser Jurassic and Proterozoic crystalline rocks and the less dense granitic rocks of the Teutonia batholith. The lowest bedrock values occur near Cima and most likely indicate where the batholith is thickest. Basin geometry is less certain where gradients in the bedrock gravity field are not constrained by gravity measurements on bedrock or by wells that penetrated bedrock.

The basin thickness results (fig. 8) indicate that thin (<1 km) basin deposits cover much of the Preserve, except for Ivanpah Valley and the Woods Mountains volcanic center. Localized areas of basin fill thicker than 500 m are predicted beneath parts of Lanfair Valley, Fenner Valley, near Kelso, Soda Lake, and southeast of Baker. The geometry of the basins in the western part of the preserve is not well constrained by data; for example, the basin southeast of Baker is constrained by one gravity measurement and the absence of measurements in the southern part of the Soda Lake area precludes an accurate definition of the basin geometry. Along the southern margin of the Mojave National Preserve, basins greater than 1 km deep are located between the Clipper and Marble Mountains, between the Marble and Bristol Mountains, and south of the Bristol Mountains. Local pockets of thicker basin fill in the Ludlow area are located over outcrops of Tertiary volcanic rocks, where our assumed density-depth function may not be accurate. Nonetheless, despite using different methods to remove the regional field, and using different density contrasts, our results for the Woods Mountains center are consistent with results from a focused study by Mickus and McCurry (1999), indicating that volcanic deposits there are 4-5 km thick.

Magnetic anomalies reflect lateral variations in the magnetization of rocks, generally caused by magnetite in rocks from the surface to mid- to lower crustal depths. These anomalies can be explained by the variations in rock type across the region. In the Mojave National Preserve and adjacent areas, aeromagnetic anomalies generally reflect crystalline basement-rock types, or Cenozoic volcanic rocks (Hendricks, 2007). Sedimentary deposits are generally only weakly magnetic and thus the magnetic data can allow us to map basement and volcanic features beneath the Cenozoic basin fill. In these cases, because of the increased distance between sensor and source, the amplitudes and gradients of the anomalies will be reduced, and the magnetic character may be different from areas where similar source rocks are exposed or near the surface. An example of this effect is the north-striking magnetic highs and magnetization boundaries over the Ivanpah Mountains that become attenuated to the south into Ivanpah Valley (figs. 7, 10).

As discussed by Hendricks (2007), three types of magnetic patterns can be related to rock type or environment, at least in those areas covered by higher-resolution aeromagnetic data. Low-amplitude (<200 nT), low-gradient magnetic highs and lows

correspond to alluvium-filled valleys and areas of predominantly Cretaceous granite, such as the Cima Dome area, Fenner Hills, and parts of Ivanpah, Fenner, and Lanfair Valleys. Intermediate- to large-amplitude (200-500 nT) magnetic highs and lows correlate with exposures of Proterozoic metamorphic rocks and Jurassic granitic rocks, such as Providence Mountains, the eastern Ivanpah Mountains, the southern Bristol Mountains, and southeast of Old Dad Mountain. Intermediate-amplitude (100-300 nT), steep-gradient, complex anomalies are present where Cenozoic volcanic rocks are exposed, such as the Cima volcanic field (fig. 2), the Piute Range, the Clipper Mountains, and the prominent magnetic low coincident with the Woods Mountains volcanic center.

Hydrologically, faults can influence groundwater-flow paths by acting either as conduits or barriers to flow. Abrupt, linear changes in magnetization are commonly the result of faulting, where faults truncate magnetic bodies, or fracturing, where alteration changes the magnetic properties of the rocks. Because of truncation and alteration of these rocks, linear magnetization boundaries can be used to estimate the distribution of faults and/or large fracture systems. North-striking faults mapped in the Providence Mountains coincide with north-striking magnetization boundaries that can then be used to map extensions of these faults where they project out onto Cenozoic sedimentary deposits. Other magnetic lineaments do not coincide with mapped faults, but can be used to infer the locations of concealed faults. One such feature, the linear northeast-striking magnetization boundary in Ivanpah Valley, coincides with the southeast margin of the Ivanpah Valley Basin as defined by gravity (fig. 10). The magnetization boundaries also highlight the structural grain within the crystalline rocks and may serve as a proxy for fracturing, an important source of permeability in generally impermeable basement rocks (Geoscience Australia, 2008), thus mapping potential groundwater pathways through and along the ranges.

Because gravity and magnetic gradients may delineate faults in the shallow crust, information from figures 5, 7, and 10 may help to locate hydrologic boundaries that are not evident from geologic maps. A preliminary comparison of the major known faults in the study area and geophysical results suggests that geophysical gradients match some of the Cenozoic faults, but few of the Mesozoic faults. Mesozoic faults include Jurassic normal faults in the Providence Mountains, Cretaceous thrust faults in the Mescal and Clark Mountain Ranges, and the latest Cretaceous normal fault along the east side of the Providence Mountains (Miller and others, 1991, Miller and others, 1996; Wells and others, 2005). These faults apparently have too shallow a dip and/or do not juxtapose rocks of differing physical properties to be imaged by the potential-field data. Cenozoic faults include Miocene normal fault complexes associated with detachment fault systems roughly along Piute Valley and Shadow Valley. The latest Cenozoic faults (Pliocene and Quaternary) include a sinistral fault extending from Kelso to Ivanpah Valley; and dextral faults in the Cima volcanic field, adjacent to Old Dad Mountain; and faults of the Eastern California Shear Zone farther west. Mesozoic faults are not evident in the magnetic patterns but are revealed by gravity gradients in a few places where rocks with different densities are juxtaposed, such as east of the Providence Mountains (fig. 5). Miocene faults are revealed by broad gravity lows in both areas of thick Miocene basinal deposits and several of the bounding normal faults are closely matched by gravity and magnetic gradients (for example, west side of Homer Mountain, west side of Ivanpah Mountains and Mescal Range, southwest side of the Avawatz Mountains). Quaternary and Pliocene faults of the eastern California Shear Zone are matched by geophysical gradients in several places, most notably near Amboy to Chambless, in places near Soda Lake and

Silver Lake, the north side of the Mesquite Hills (fig. 2), and the west side of the McCullough Range and Lucy Gray Mountains (figs. 5, 10).

Conclusions and Recommendations

New and compiled gravity data provide constraints on basin geometry of the Mojave National Preserve and adjacent areas, suggesting that much of the Preserve is underlain by relatively thin (<1 km) Cenozoic deposits, except for Ivanpah Valley and the Woods Mountains volcanic center that reach depths of >3 km. Localized, deeper areas of basin fill are predicted beneath parts of Lanfair Valley, Fenner Valley, near Kelso and southeast of Baker. The area east of Baker, however, is based on a gravity low constrained by a single gravity station. The basin inversion results for this area, and other areas in the western part of the Preserve, would be improved with additional gravity data.

Significant gravity variations arise from density contrasts within the pre-Cenozoic bedrock, with high values generally over areas of exposed Proterozoic and Jurassic rocks and low values over the lower-density Teutonia batholith. Because of the large gravity variations over pre-Cenozoic bedrock, the basin inversion results could be improved by additional constraints on the bedrock gravity, such as wells, additional measurements on bedrock, and by additional geophysical data on depth to bedrock. Additional data on bedrock would improve the separation of the gravity field into the basement and basin components. Given the expense and invasiveness of drilling wells, other geophysical methods (for example, electrical or seismic methods) would provide much needed independent control on depth to bedrock.

Aeromagnetic data can be used to map structure and lithologic contrasts within the crystalline basement rocks and Cenozoic volcanic rocks. These data can be used to extend mapped faults into covered areas and to serve as a proxy for fracturing within the generally impermeable crystalline basement rocks. These data may help identify potential flow paths across the ranges.

References Cited

- Acord, John, 1989, A gravity study of the Soda-Avawatz fault zone, San Bernardino County, California: Bakersfield, California State University, master's thesis, 86 p.
- Barnes, D.F., Oliver, H.W., and Robbins, S.L., 1969, Standardization of gravimeter calibrations in the Geological Survey: *Eos, Transactions, American Geophysical Union*, v. 50, no. 10, p. 626-627.
- Black, W.E., 1997, Seismic reflection survey, Cadiz Valley, Cadiz, California: Report prepared for the Cadiz Land Company, San Bernardino, Calif., 23 p.
- Blakely, R.J., 1995, Potential theory in gravity and magnetic applications: New York, Cambridge University Press 441 p.
- Blakely, R.J., and Simpson, R.W., 1986, Approximating edges of source bodies from magnetic or gravity anomalies: *Geophysics*, v. 51, p. 1494-1498.
- Briggs, I.C., 1974, Machine contouring using minimum curvature: *Geophysics*, v. 39, p. 39-48.
- Calzia, J.P., 1991a, Geophysical, lithologic, and water quality data from Broadwell Dry Lake, San Bernardino County, California: U.S. Geological Survey Open-File Report 91-267.

- Calzia, J.P., 1991b, Geophysical, lithologic, and water quality data from Ivanpah Valley, San Bernardino County, California: U.S. Geological Survey Open-File Report 91-265.
- Calzia, J.P., 1991c, Geophysical, lithologic, and water quality data from Soda Dry Lake, San Bernardino County, California: U.S. Geological Survey Open-File Report 91-266.
- Carlisle, C.L., 1982, The subsurface structure of the Ivanpah Valley, California, as determined by geophysical measurements: Santa Barbara, University of California, master's thesis, 90 p.
- Carlisle, C.L., Luyendyk, B.P., and McPherron, R.L., 1980, Geophysical survey in the Ivanpah Valley and vicinity, eastern Mojave Desert, California *in* Fife, D.E., and Brown, A.R., eds., *Geology and mineral wealth of the California desert*: Santa Ana, California, South Coast Geological Society, p. 485-494.
- Chapman, R.H., Joseph, S.E., and Campbell, L.G., 1986, Magnetic exploration for skarn deposits, Ivanpah mining district, San Bernardino County, California: *California Geology*, v. 39, p. 171-178.
- Division of Oil and Gas, 1980, Oil and gas prospect wells drilled in California through 1980: California Division of Oil and Gas Publication TRO 1, 258 p.
- Gardner, G.H., Gardner, L.W., and Gregory, A.R., 1974, Formation velocity and density; the diagnostic basis for stratigraphic traps: *Geophysics*, v. 39, p. 770-780.
- Geolife, Inc., 1979, Aerial radiometric and magnetic survey, Trona National Topographic Map, California: U.S. Department of Energy, Grand Junction Office Report GJBX-065(79), 2 vols.
- Geoscience Australia, 2008, Chapter 8—Groundwater in fractured rock aquifers *in* Assessment of groundwater resources in the Broken Hill region, p. 89-97. [available at <http://www.environment.gov.au/water/publications/environmental/groundwater/broken-hill.html>, last accessed April 17, 2009].
- Godson, R.H., and Plouff, Donald, 1988, BOUGUER version 1.0, a microcomputer gravity–terrain–correction program: U.S. Geological Survey Open-File Report 88-644-A, Documentation, 22 p.; 88-644-B, tables, 61 p., 88-644-C.
- Grauch, V.J.S., and Cordell, L., 1987, Limitations of determining density or magnetic boundaries from the horizontal gradient of gravity or pseudogravity data: *Geophysics*, 52, p. 118-121.
- Hayford, J.F., and Bowie, William, 1912, The effect of topography and isostatic compensation upon the intensity of gravity: U.S. Coast and Geodetic Survey Special Publication no. 10, 132 p.
- Hendricks, J.D., 2007, Geophysics *in* Theodore, Ted, ed., *Geology and mineral resources of the East Mojave National Scenic Area, San Bernardino County, California*: U.S. Geological Survey Bulletin 2160, p. 81-87, [available at <http://pubs.usgs.gov/bul/b2160/>, last accessed February 2, 2009].
- High Life Helicopters, Inc., and QEB, Inc., 1980, Airborne gamma-ray spectrometer and magnetometer survey, Los Angeles Quadrangle, San Bernardino Quadrangle, Santa Ana Quadrangle, San Diego Quadrangle, California: U.S. Department of Energy, Grand Junction Office Report GJBX-214(80), 5 vols.
- International Union of Geodesy and Geophysics, 1971, Geodetic reference system 1967: International Association of Geodesy Special Publication no. 3, 116 p.
- Jachens, R.C., and Moring, B.C., 1990, Maps of the thickness of Cenozoic deposits and the isostatic gravity over basement for Nevada: U.S. Geological Survey Open-File Report 90-404, 15 p.

- Jachens, R.C., and Roberts, C.W., 1981, Documentation of a FORTRAN program, 'isocomp', for computing isostatic residual gravity: U.S. Geological Open-File Report 81-574, 26 p.
- Jennings, C.W., Strand, R.G., and Rogers, T.H., 1977, Geologic map of California: California Division of Mines and Geology, scale 1:750,000.
- Jennings, C.W., 1994, Fault activity map of California: California Division of Mines and Geology Data Map 6, scale 1:750,000.
- Mariano, John, Jachens, R.C., and Miller, R.J., 2007a, Isostatic residual gravity map of the East Mojave National Scenic Area, California *in* Theodore, Ted, ed., Geology and mineral resources of the East Mojave National Scenic Area, San Bernardino County, California: U.S. Geological Survey Bulletin 2160, [<http://pubs.usgs.gov/bul/b2160/>, last accessed February 2, 2009].
- Mariano, John, Jachens, R.C., and Miller, R.J., 2007b, Aeromagnetic map of the East Mojave National Scenic Area, California *in* Theodore, T.G., ed., Geology and mineral resources of the East Mojave National Scenic Area, San Bernardino County, California: U.S. Geological Survey Bulletin 2160. [available at <http://pubs.usgs.gov/bul/b2160/>, last accessed February 2, 2009].
- McCurry, M., 1988, Geology and petrology of the Woods Mountains volcanic center, southeastern California: *Journal of Geophysical Research*, v. 93, p. 835-855.
- Mickus, K.L., and McCurry, M., 1999, Gravity and aeromagnetic constraints on the structure of the Woods Mountains volcanic center, southeastern California: *Bulletin of Volcanology*, v. 60, p. 523-533.
- Miller, D.M., 1995, Characteristics, age, and tectonic implications of the Mid Hills pediment: *San Bernardino County Museum Association Quarterly*, v. 42, no. 3, p. 69-74.
- Miller, D.M., and Wooden, J.L., 1993, Geologic map of the New York Mountains area, California and Nevada: U.S. Geological Survey Open File Report 93-198, 10 p., scale 1:50,000.
- Miller, D.M., Frisken, J.G., Jachens, R.C., and Gese, D.D., 1986, Mineral resources of the Castle Peaks Wilderness Study Area, San Bernardino County, California: U.S. Geological Survey Bulletin 1713-A, 17 p.
- Miller, D.M., Miller, R.J., Nielson, J.E., Wilshire, H.G., Howard, K.A., and Stone, Paul, 1991, Preliminary geologic map of the East Mojave National Scenic Area, California: U.S. Geological Survey Open-File Report 91-435, scale 1:100,000, 7 p.
- Miller, D.M., Miller, R.J., Nielsen, J.E., Wilshire, H.G., Howard, K.A., and Stone, Paul, 2007a, Geologic map of the East Mojave National Scenic Area, California *in* Theodore, Ted, ed., Geology and mineral resources of the East Mojave National Scenic Area, San Bernardino County, California: U.S. Geological Survey Bulletin 2160, [available at <http://pubs.usgs.gov/bul/b2160/>, last accessed February 2, 2009].
- Miller, D.M., Dudash, S.L., Green, H.L., Lidke, D.J., Amoroso, Lee, Phelps, G.A., and Schmidt, K.M., 2007b, A new Quaternary view of northern Mojave Desert tectonics suggests changing fault patterns during the late Pleisocene in Miller, D.M., and Valin, Z.C., eds. *Geomorphology and Tectonics at the Intersection of Silurian and Death Valleys, Southern California*: U.S. Geological Survey Open-File Report 2007-1424, p. 157-171, [available at <http://pubs.usgs.gov/of/2007/1424/> last accessed February 2, 2009].

- Miller, D.M., Wells, M.L., Dewitt, E., Walker, J.D., and Nakata, J.K., 1996, Late Cretaceous extensional fault system across the northeastern Mojave Desert, *in* Reynolds, R.E., and Reynolds, J., compilers, Punctuated chaos in the northeastern Mojave Desert: San Bernardino County Museum Quarterly, v. 43, no. 1/2, p. 77-84.
- Morelli, C., ed, 1974, The International Gravity Standardization Net 1971: International Association of Geodesy Special Publication no. 4, 194 p.
- Moyle, W.R., 1967, Water wells and springs in Bristol, Broadwell, Cadiz, Danby, and Lavic Valleys in vicinity: California Department of Water Resources Bulletin 91-14, 17 p.
- Moyle, W.R., 1972, Water wells and springs in Ivanpah Valley, San Bernardino County, California: California Department of Water Resources Bulletin no. 91-21.
- Oliver, H.W., Chuchel, B.A., and Saltus, R.W., 1986, Aeromagnetic map of Nevada, Kingman sheet: Nevada Bureau of Mines and Geology, scale 1:250,000.
- Plouff, Donald, 1966, Digital terrain corrections based on geographic coordinates [abs.]: Geophysics, v. 31, no. 6, p. 1,208.
- Plouff, Donald, 1977, Preliminary documentation for a FORTRAN program to compute gravity terrain corrections based on topography digitized on a geographic grid: U.S. Geological Survey Open-File Report 77-535, 45 p.
- Roberts, C.W., and Jachens, R.C., 1986, High-precision gravity stations for monitoring vertical crustal motion in southern California: U.S. Geological Survey Open-File Report 86-44, 76 p.
- Roberts, C.W., and Jachens, R.C., 1999, Preliminary aeromagnetic map of California: U.S. Geological Survey Open-File Report 99-440, 14 p., [available at <http://geopubs.wr.usgs.gov/open-file/of99-440/>, last accessed December 2, 2008].
- Roberts, C.R., Jachens, R.C., and Oliver, H.W., 1990, Isostatic residual gravity map of California and offshore southern California: California Division of Mines and Geology California Geologic Data Map No. 7, scale 1:750,000.
- Rush, F.E., and Huxel, C.J., Jr., 1966, Ground-water appraisal of the Eldorado-Piute Valley area, Nevada and California: Nevada Department of Conservation and Natural Resources Water-Resources Reconnaissance Report 36, 29 p., scale 1:250,000.
- Schmidt, K.M., and Webb, R.H., 2001, Researchers consider U.S. Southwest's response to warmer, drier climate: EOS, Transactions, American Geophysical Union, v. 82, no. 41, p. 475-478.
- Shearer, Peter, Hauksson, Egill, and Lin, Guoqing, 2005, Southern California hypocenter relocation with waveform cross-correlation, part 2—Results using source-specific station terms and cluster analysis: Bulletin of the Seismological Society of America, v. 95, p. 904-915.
- Simpson, R.W., Jachens, R.C., Blakely, R.J., and Saltus, R.W., 1986, A new isostatic residual gravity map of the conterminous United States with a discussion on the significance of isostatic residual anomalies: Journal of Geophysical Research, v. 91, p. 8348-8372.
- Swick, C.A., 1942, Pendulum gravity measurements and isostatic reductions: U.S. Coast and Geodetic Survey Special Publication 232, 82 p.
- Theodore, T.G., ed., 2007, Geology and mineral resources of the East Mojave National Scenic Area, San Bernardino County, California: U.S. Geological Survey Bulletin 2160, 274 p., [available at <http://pubs.usgs.gov/bul/b2160/>, last accessed February 10, 2009].

- Thompson, D.G., 1929, The Mohave Desert region, California, a geographic, geologic, and hydrographic reconnaissance: U.S. Geological Survey Water-Supply Paper 578, 759 p.
- Tucci, Patrick, Schmoker, J.W., and Robbins, S.L., 1982, Borehole-gravity surveys in basin-fill deposits of central and southern Arizona: U.S. Geological Survey Open-File Report 82-473, 24 p.
- University of Nevada-Reno, 1999, Historical catalog (1952-1999), Nevada Seismological Laboratory Earthquake catalog search, [available at <http://www.seismo.unr.edu/Catalog/catalog-search.html>, last accessed December 20, 1998].
- U.S. Geological Survey, 1979, Aeromagnetic map of southern Nevada: U.S. Geological Survey Open-File Report 79-1474, scale 1:250,000.
- U.S. Geological Survey, 1981, Aeromagnetic map of the Needles 1 by 2 degree quadrangle, California and Arizona: U.S. Geological Survey Open-File Report 81-085, scale 1:250,000.
- U.S. Geological Survey, 1983, Aeromagnetic map of the Kingman-Trona area, California: U.S. Geological Survey Open-File Report 83-663, scale 1:250,000.
- U.S. Geological Survey, 2009, Geographic Names Information Systems, [available at <http://geonames.usgs.gov/pls/gnispublic>, last accessed February 2, 2009].
- Webring, M.W., 1981, MINC—A gridding program based on minimum curvature: U.S. Geological Survey Open File Report 81-1224, 43 p.
- Wells, M.L., Beyene, M.A., Spell, T.L., Kula, J.L., Miller, D.M., and Zanetti, K.A., 2005, The Pinto shear zone; a Laramide synconvergent extensional shear zone in the Mojave Desert region of the southwestern United States: *Journal of Structural Geology*, v. 27, p. 1697-1720.
- Wilshire, H.G., Frisken, J.G., Jachens, R.C., Prose, D.V., Rumsey, C.M., and McMahan, A.B., 1987, Mineral resources of the Cinder Cones Wilderness Study Area, San Bernardino County, California: U.S. Geological Survey Bulletin 1712-B, 13 p.

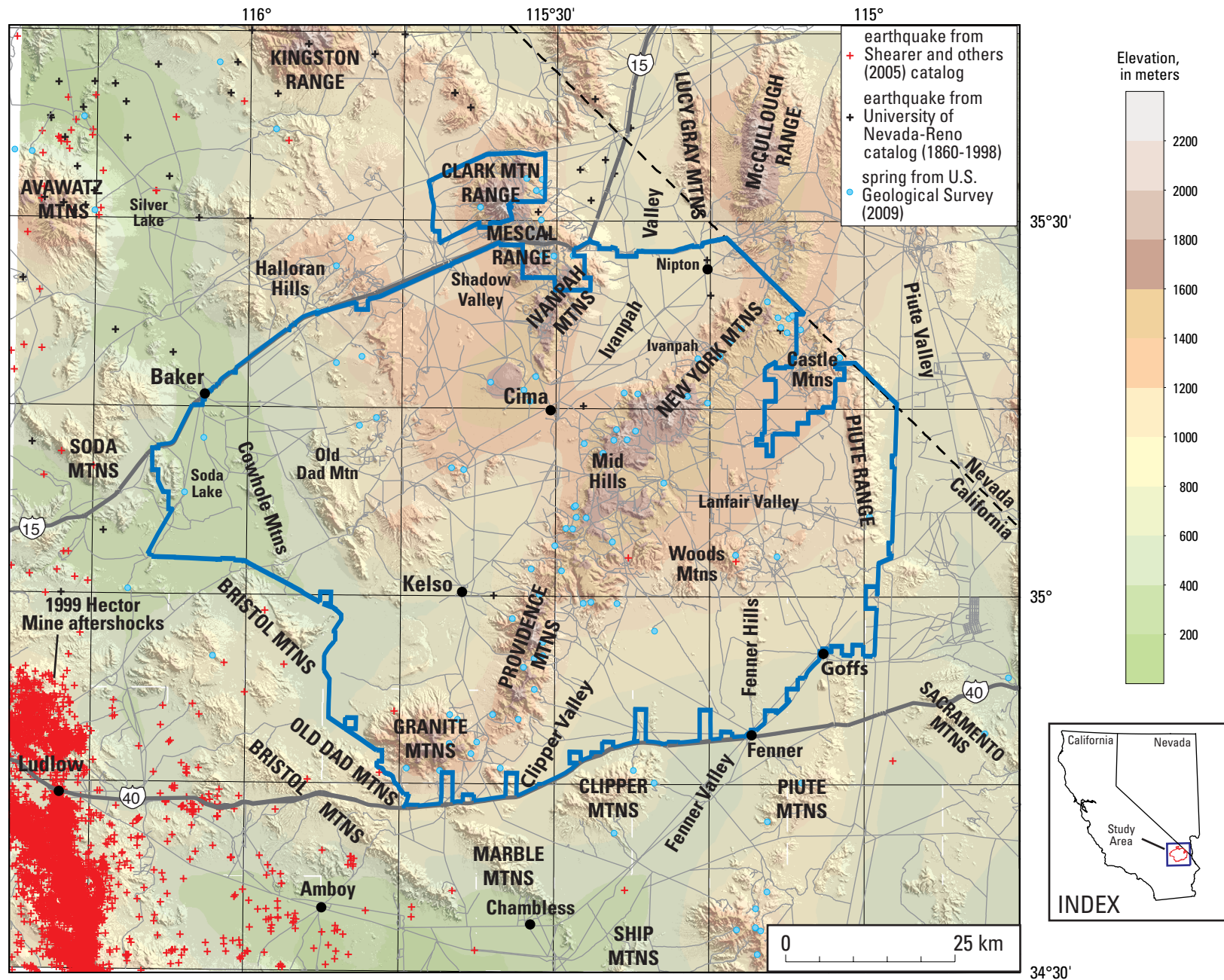


Figure 1. Index map of the study area, which consists of the Mojave National Preserve (outlined in blue) and adjacent areas, California and Nevada. Gray lines, roads from U.S. Geological Survey 1:100,000-scale topographic maps.

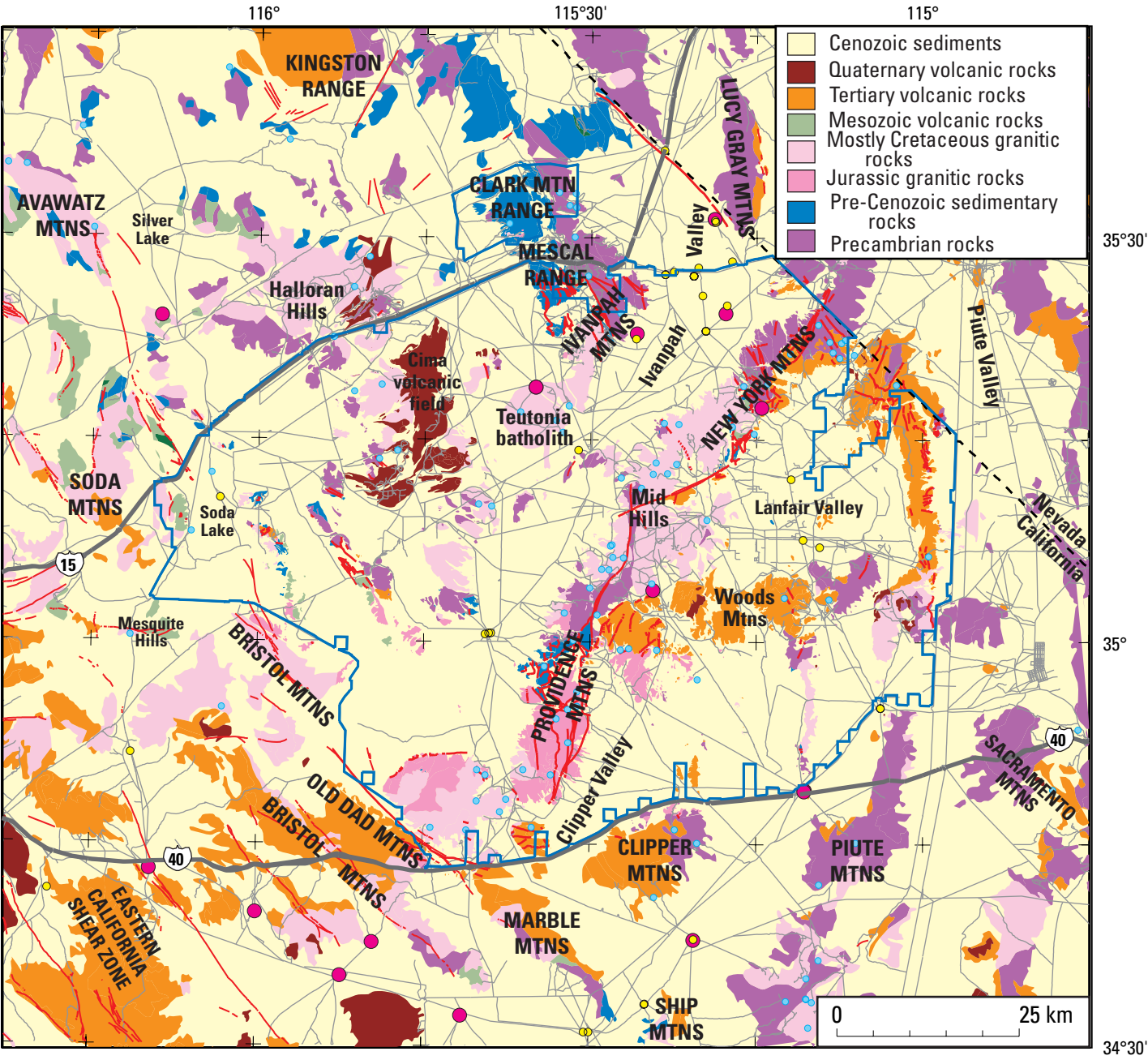


Figure 2. Simplified geologic map of the Mojave National Preserve (outlined in blue) and adjacent areas. Geology within the Preserve is modified after Miller and others (2007a); geology outside of the Preserve is modified from Jennings (1977). Magenta circles, drill holes interpreted to have encountered pre-Cenozoic rocks; yellow circles, drill holes that did not encounter pre-Cenozoic rocks; red lines, faults from Miller and others (2007a, b); and Jennings (1994); blue circles, spring locations.

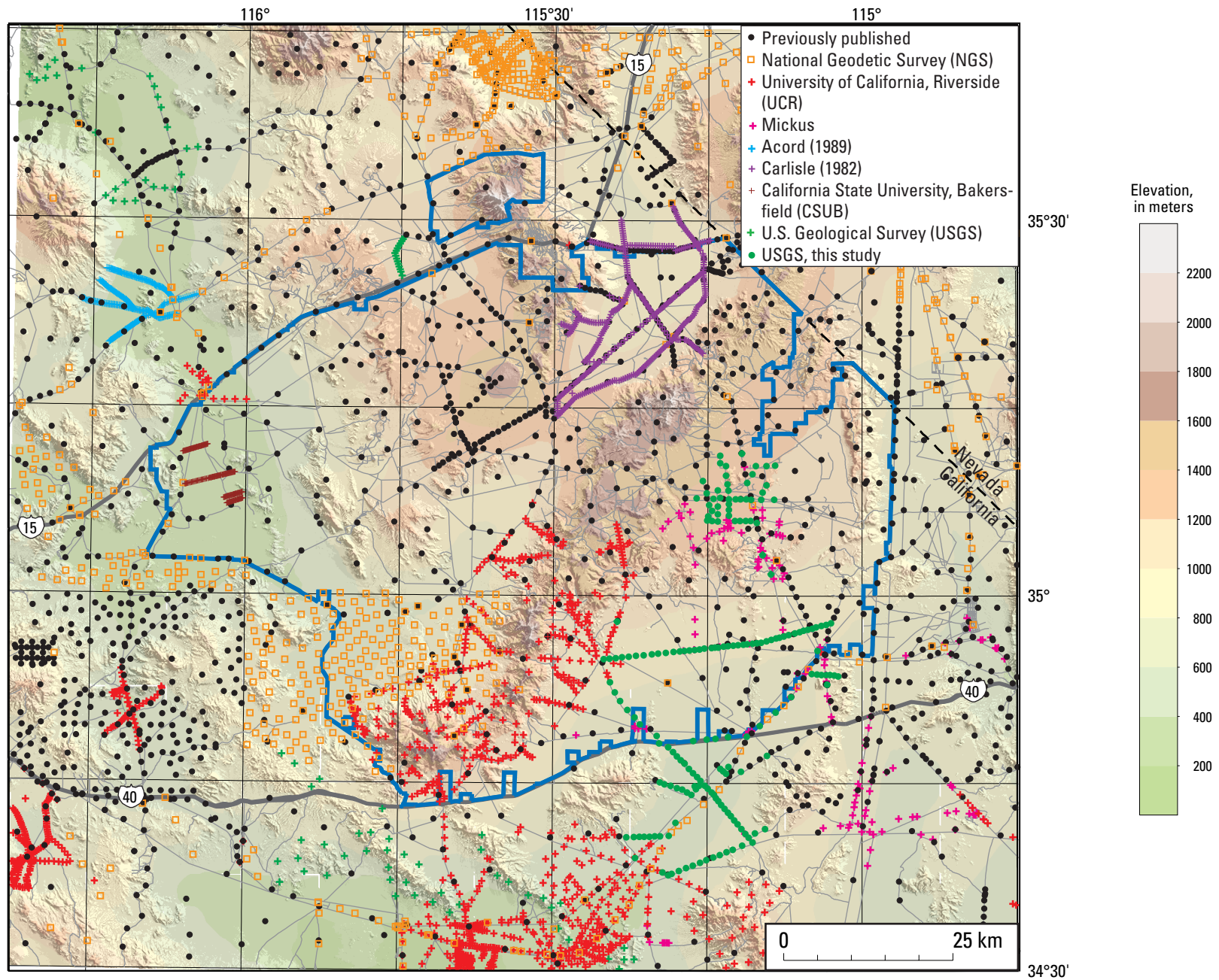


Figure 3. Map of gravity measurements in the Mojave National Preserve (outlined in blue) and adjacent areas, California and Nevada.



Figure 4. A, Google image of Ludlow, California showing location of secondary base station in Ludlow relative to Interstate 40. B, Photograph of secondary base station located at southeast corner of concrete walkway along the Ludlow Motel. View is to the north towards Ludlow Road and Interstate 40.

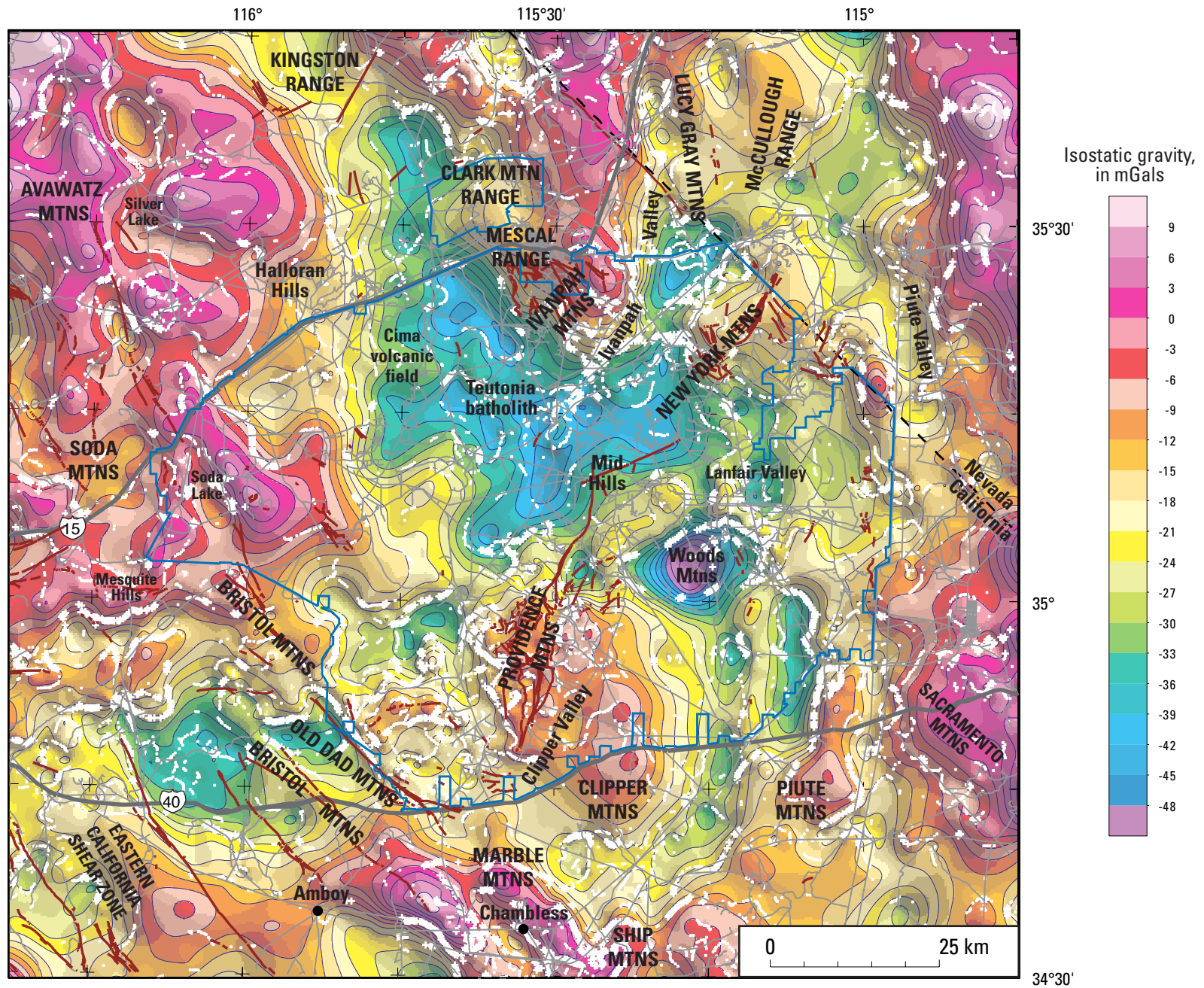


Figure 5. Isostatic gravity map of the Mojave National Preserve (outlined in blue) and adjacent areas, California and Nevada. Contour interval, 3 mGal. White crosses show location of maximum horizontal gravity gradient with larger crosses denoting gradient amplitudes greater than the mean gradient and smaller crosses denoting gradient amplitudes less than the mean gradient. Brown lines are faults.

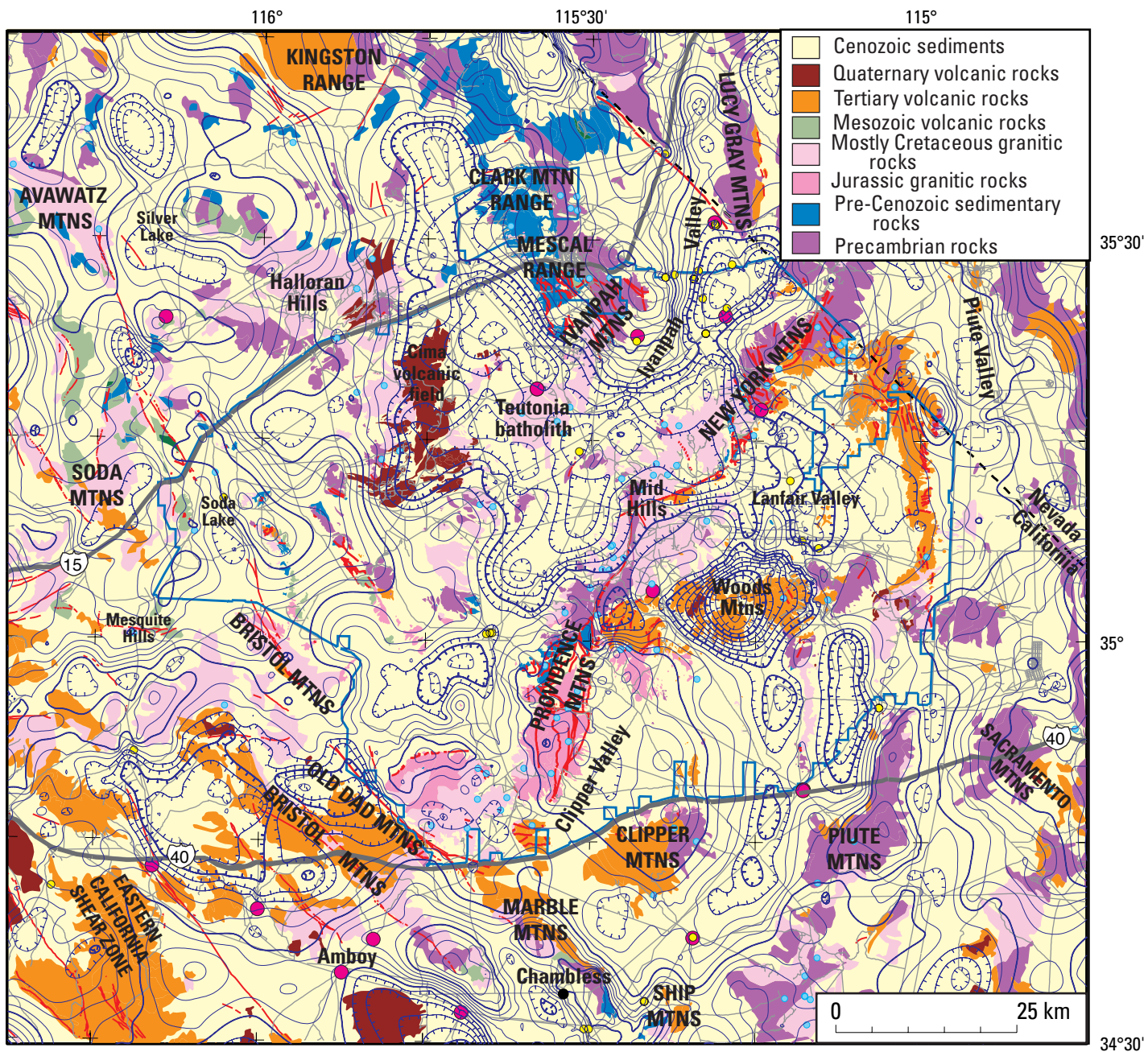


Figure 6. Isostatic gravity contours (from figure 5) on simplified geologic map of the Mojave National Preserve (outlined in blue) and adjacent areas, California and Nevada. Hachures denote gravity lows. See figure 2 for explanation of geology. Magenta circles, drill holes interpreted to have encountered pre-Cenozoic rocks; yellow circles, drill holes that did not encounter pre-Cenozoic rocks; red lines, faults from Miller and others (2007a, b) and Jennings (1994).

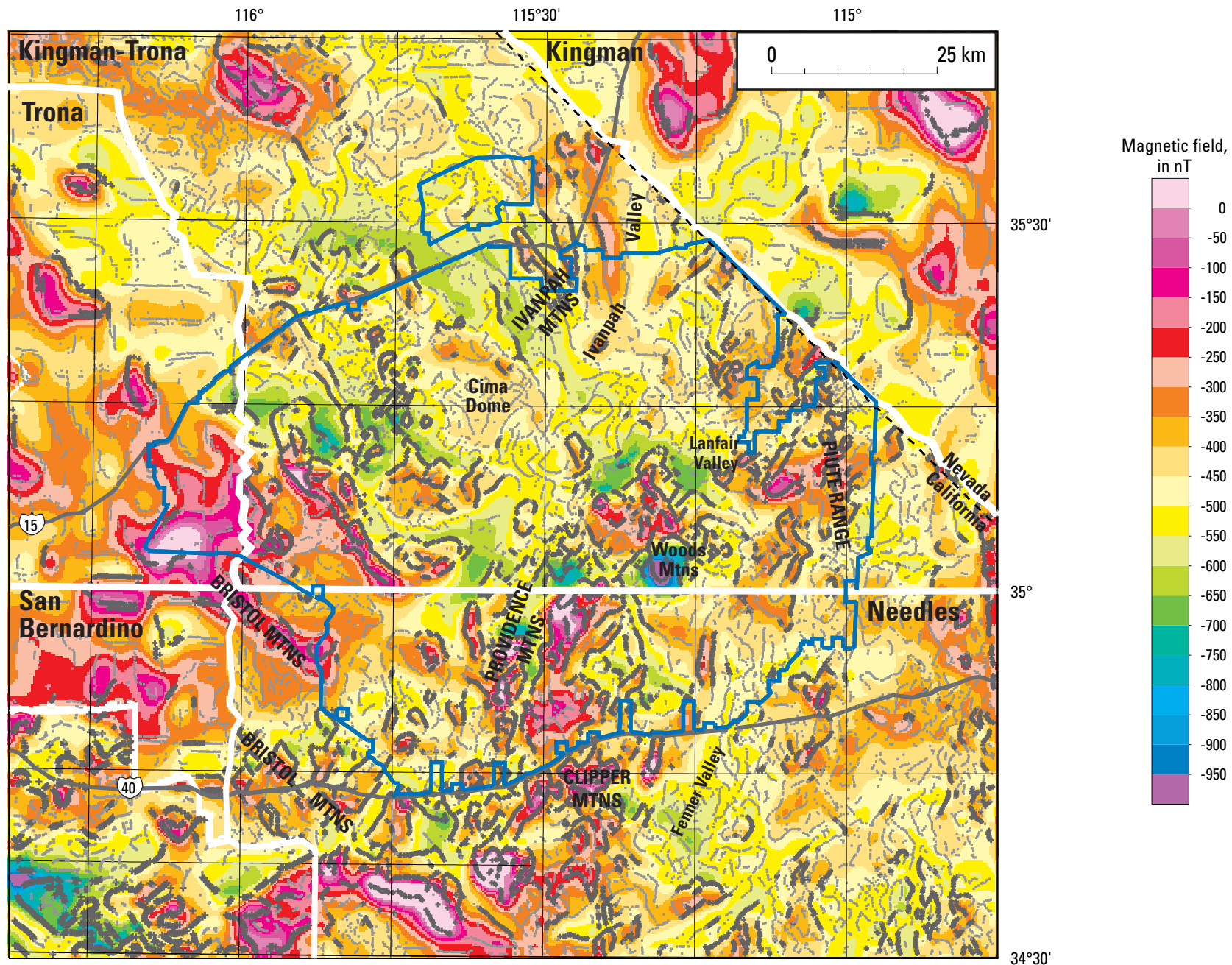


Figure 7. Aeromagnetic map of the Mojave National Preserve (outlined in blue) and adjacent area, California and Nevada. White lines denote survey boundaries; labels denote survey names. See table 1 for survey specifications. Dark gray and light gray spots denote magnetization boundaries, with dark gray denoting gradient amplitudes greater than the mean gradient and light gray denoting gradient amplitudes less than the mean gradient.

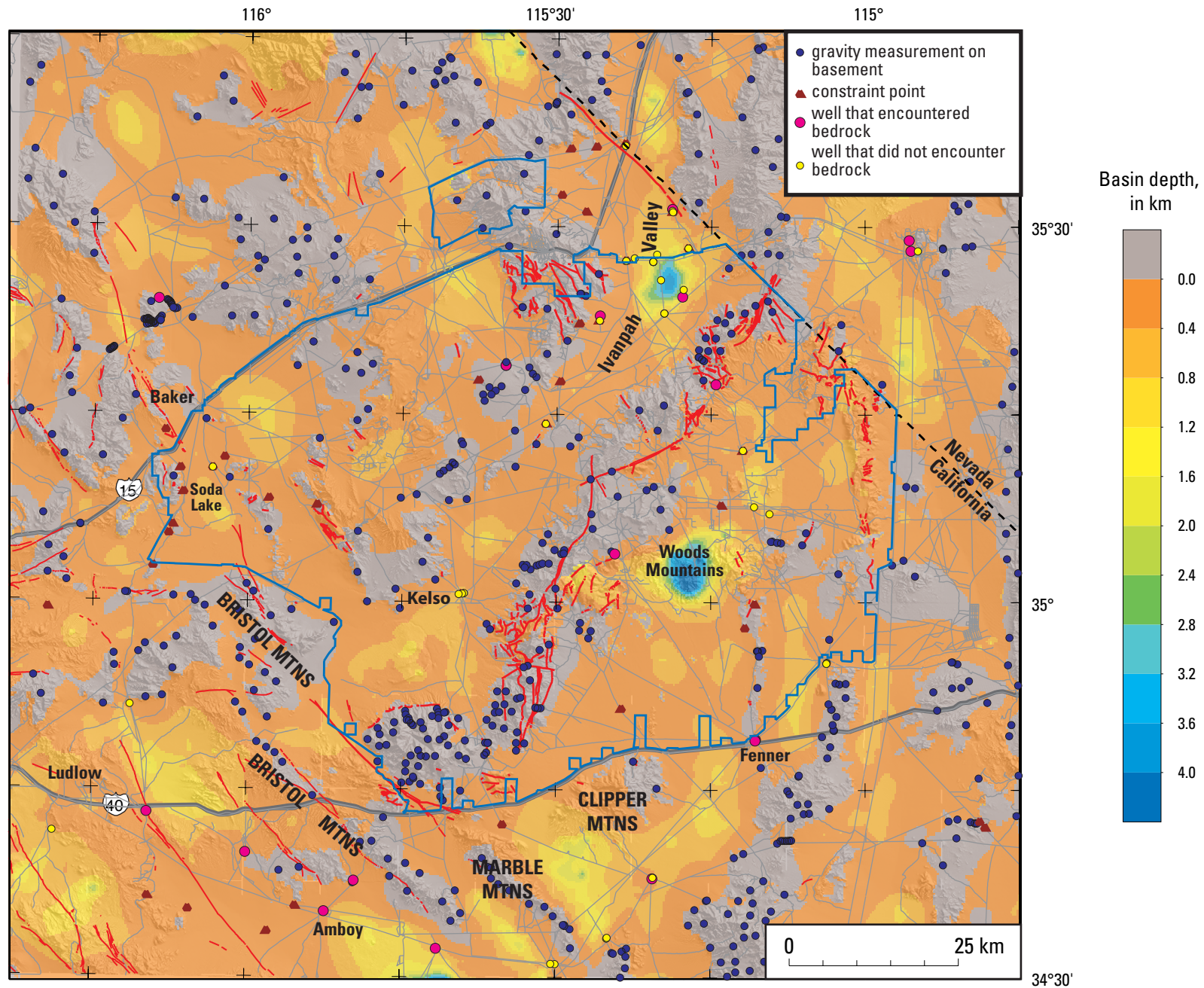


Figure 8. Basin depth from inversion of gravity data for the Mojave National Preserve (outlined in blue) and adjacent areas, California and Nevada.

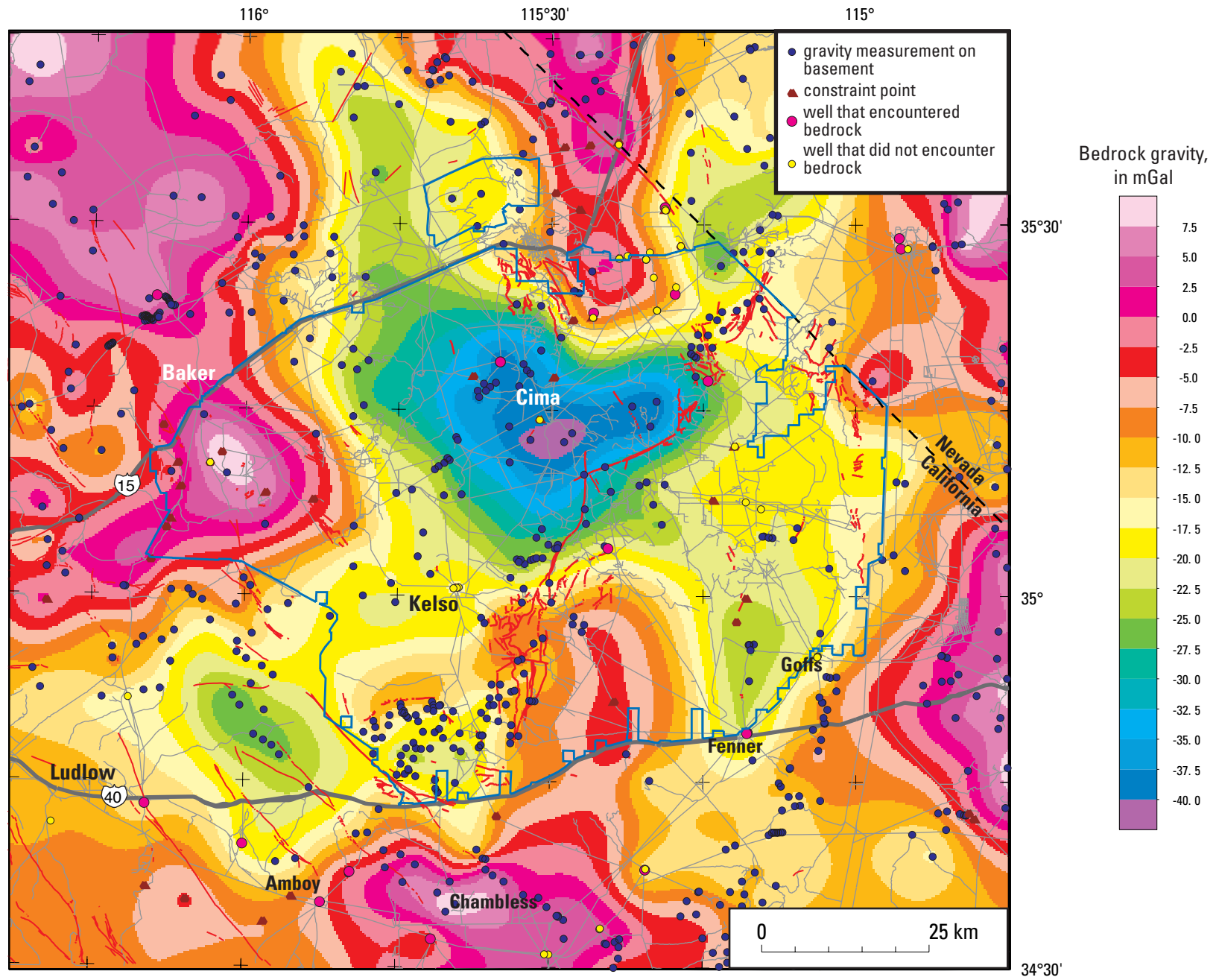


Figure 9. Bedrock gravity of the Mojave National Preserve (outlined in blue) and adjacent areas, California and Nevada. Faults, red lines.

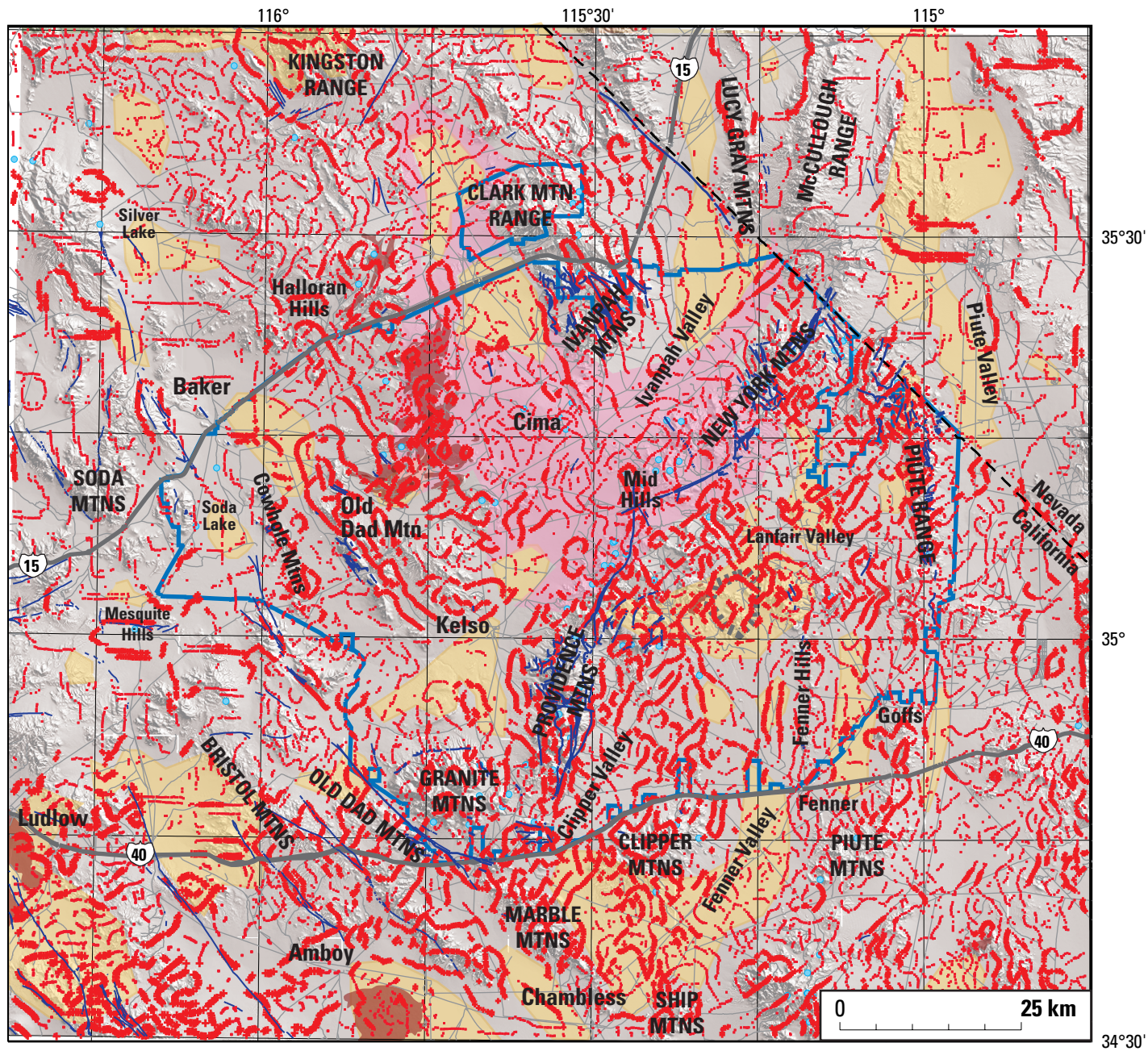


Figure 10. Map showing magnetization boundaries (red circles and dots), basins more than 400 m deep (buff areas) from figure 8, Quaternary volcanic rocks (brown areas), and areas underlain by the Teutonia batholith (pink areas) plotted on shaded-relief topographic map of the Mojave National Preserve (outlined in blue) and adjacent areas, California and Nevada. Faults, dark blue lines. Bold, dashed gray line south of Lanfair Valley outlines the extent of the Woods Mountains volcanic center.